THE JOURNAL OF PHYSICAL CHEMISTRY B

Article

pubs.acs.org/JPCB

Electron Transfer in *Rhodobacter sphaeroides* Reaction Centers Containing Zn-Bacteriochlorophylls: A Hole-Burning Study

Bhanu Neupane,[†] Paul Jaschke,[§] Rafael Saer,[§] J. Thomas Beatty,[§] Mike Reppert,[⊥] and Ryszard Jankowiak*[,†,‡]

[†]Department of Chemistry and [‡]Department of Physics, Kansas State University, Manhattan, Kansas 66506, United States

[§]Department of Microbiology & Immunology, University of British Columbia, Vancouver, BC, Canada

[⊥]Department of Chemistry, Massachusetts Institute of Technology, Cambridge, Massachusetts, United States

ABSTRACT: Nonresonant and resonant transient, photochemical hole-burned (HB) spectra are presented for primary electron donor states of a novel bacterial reaction center (Zn-RC) of *Rhodobacter sphaeroides*, containing six Zn-bacteriochlorophylls (Zn-BChls). A "Zn-β-RC" in which the Zn-BChl in the bacteriopheophytin (BPhe)-binding site on the A side (H_A) has the Zn penta-coordinated, was also studied. The fifth ligand comes from a histidine introduced by site-directed mutagenesis. Formation of the $P^+Q_A^-$ state was observed in both types of RC, although under identical experimental conditions a significantly deeper P_ band (corresponding to the lower-energy, special pair, excitonic component) was revealed in the Zn-RC. Assuming a similar lifetime of the $P^+Q_A^-$ state, the quantum yield of $P^+Q_A^-$ formation decreased by ~60% in the Zn-β-RC (compared to the Zn-RC), as was seen in a comparison of analogous (Mg) BChl-containing wild type and β-RCs of *Rb. sphaeroides* [Kirmaier et al. *Science* **1991**, *251*, 922]. However, the average (weakly frequency-dependent) low-temperature electron transfer (ET) rates of the Zn-RC and Zn-β-RC (measured from zero phonon holes in resonant transient HB spectra) were both ~1 ps and similar to a rate previously measured in the *Rb. sphaeroides* native RC [Johnson et al. *J. Phys. Chem.* **1989**, *93*, 5953]. Electron transfer rates observed in this work on the Zn-RC yielded a P870* decay rate in good agreement with recent room-temperature, time-domain data [Lin et al. *Proc. Natl. Acad. Sci.* **2009**, *106*, 8537]. A lack of correlation observed between the holes near 810 and 883 nm, accounting for electrochromically induced shifts of the Zn-BChl transitions in the $B_{A,B}$ and $H_{A,B}$ binding sites, produced by formation of the $P^+BHQ_A^-$ state, indicates that the 810 nm bleach does not correspond to the P_+ (upper excitonic component of the dimer) band and is mostly contributed to by a shift of the B_B absorption band. ZPH-action spectra indicated inhomogeneous broadening (Γ_{inh}) of ~110 cm^{-1} (Zn-RC) and ~130 cm^{-1} (Zn-β-RC). Experimentally determined Γ_{inh} decreased the number of variables in theoretical fits of the absorption and frequency-dependent shapes of resonant HB spectra, leading to more reliable Huang–Rhys factors for both low-frequency phonons and a pseudolocalized phonon, ω_{SP}, often referred to as the special pair marker mode.

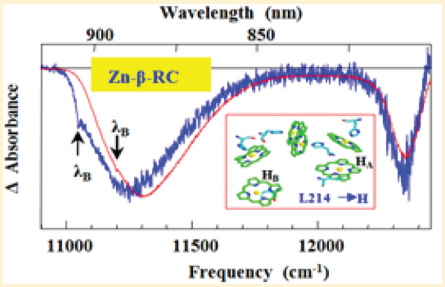

1. INTRODUCTION

The purple nonsulfur bacterium *Rhodobacter (Rb.) sphaeroides* is an extremely useful system for studying photosynthetic electron transfer (ET). The core of the relatively simple photosynthetic apparatus in this bacterium is a dimer of a reaction center (RC) complex surrounded by the light-harvesting 1 complex (LH1) and the PufX protein.[1−3] The bacterial RC (BRC) contains three proteins called H, M, and L; the structurally similar RC M and L proteins consist of five transmembrane helices with pseudo 2-fold symmetry, whereas the RC H protein has only one transmembrane helix and a large cytoplasmic domain.[4] The type 2 RC of *Rb. sphaeroides* contains a "special pair" bacteriochlorophyll *a* (BChl) dimer (sometimes called "P") bound by RC M and L proteins on the periplasmic side of the membrane. The special pair is flanked by two accessory BChls bound to RC L (in the B_A site) and RC M (in the B_B site), which are the periplasmic ends of two cofactor branches called A and B (predicted cofactor arrangement in the Zn-RC is shown in Figure 1A). Two bacteriopheophytin *a* (BPhe) molecules (in the H_A and H_B sites) are located between the accessory BChls and two quinones (Q_A and Q_B), which are bound near the cytoplasmic side of the RC. An iron (Fe^{2+}) atom is located between Q_A and Q_B, and a carotenoid is bound near the special pair on the B-branch side.[5] Electrons are transferred through the A-branch pigments, from the special pair through the monomeric BChl in the B_A position[6] and then to the BPhe in the H_A-site, before passing on to the Q_A and finally the Q_B quinone.[7]

The relative redox energies of the different pigments of the *Rb. sphaeroides* RC are among the best understood of any photosynthetic complex, due to their simplicity and ease of spectroscopic measurement.[8−11] The redox midpoint potentials of each step in the A-branch result in a series of energetically favorable downhill reactions, and the times for electron transfer

Received: January 10, 2012
Revised: February 10, 2012
Published: February 10, 2012

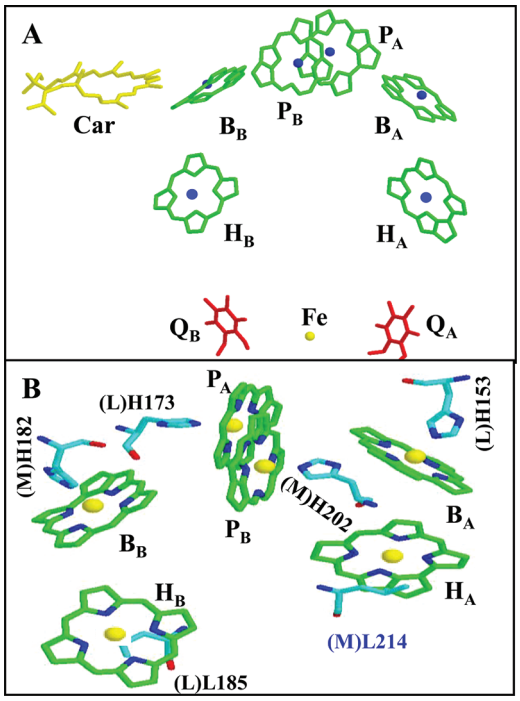

Figure 1. Predicted cofactor arrangement in the Zn-RC, based on 2.0 Å crystal structure of the WT-RC from *Rb. sphaeroides*, PDB ID 3I4D. (A) Cofactors are shown in different colors: carotenoid (yellow), Zn-BChls (green; Zn atoms shown as blue sphere), and ubiquinones in red. (B) Close-up view of Zn-BChls. Atoms are color-coded: carbon green, nitrogen blue, and magnesium yellow. Four histidine residues H173, H202, H153, and H182 (that ligate the BChl Mg^{2+} in the WT-RC) and two leucine residues L214 and L185 (that are closer to H_A and H_B, respectively) are also shown. The letter L and M (in parentheses) refer to the protein chains to which the residues belong. All residue atoms are color-coded: nitrogen blue, oxygen red, and carbon cyan. In both frames, the alkyl tail of ubiquinones and Zn-Bchls and all other side chains of Zn-BChls are truncated for clarity.

(ET) from P* → H_A → Q_A → Q_B at room temperature are 3 ps, 200 ps, and 200 μs, respectively.[12] These times reflect the magnitude differences in redox potential of the pigments involved, because this trait is the fundamental driving force of the reaction, although recent work has suggested that protein dynamics also plays a significant role in the overall kinetics of the reaction.[13]

Recently, it was discovered that a mutant of *Rb. sphaeroides* contains a modified BChl biosynthetic pathway that causes it to produce a different type of BChl, where the central Mg^{2+} has been replaced by Zn^{2+} (Zn-BChl), as well as ceasing production of BPhe.[14,15] In this mutant, Zn-BChl is assembled into the RC and LH1 complexes in place of the normal (Mg-)BChl and BPhe.[14,16] A more detailed investigation of the so-called Zn-RC, using low-temperature spectroscopy, indicated that it contains 6 Zn-BChl in the P-, $B_{A,B}$- and $H_{A,B}$-sites in place of the four BChls and two BPhes.[16] The change in the cofactor in the H_A-site from a BPhe in the wild type RC (WT-RC) to a Zn-BChl in the Zn-RC mimics a site-directed mutant of the RC, called the β mutant RC, that caused a BChl to take the place of BPhe in the H_A-site.[12] This β mutant RC caused a reduction in ET efficiency from P to H_A to ~50% of the WT-RC, thought to be caused by a converging of the redox-potentials of the B_A and H_A cofactors, due to the change in the H_A cofactor from BPhe to BChl. Therefore it was surprising that the ET reactions of the Zn-RC were found to be nearly identical to those of the WT-RC, despite the Zn-RC cofactor arrangement (with a Zn-BChl in the H_A-site), more closely resembling the β mutant RC than the WT-RC.[16]

The preservation of efficient ET in the Zn-RC was ascribed to the coordination state of the Zn-BChl bound to the H_A-site. In the WT-RC and Zn-RC P- and $B_{A,B}$-sites, Mg- and Zn-BChl are both penta-coordinated: four ligands come from the BChl molecule itself and the fifth from the RC protein which provides a His residue in an axial position to the central metal;[4,17] see Figure 1B. In the WT-RC the H_A-site binds BPhe, which does not contain a metal ion and possesses a more positive redox potential than B_A-BChl. It was suggested that, in the Zn-RC, the Zn-BChl bound to the H_A-site is not penta- but tetra-coordinated, because a fifth coordinating ligand (His residue) is absent in the H_A-site. Thus, it was thought that the tetra-coordinated Zn-BChl would have a more positive redox potential and would be more similar to BPhe than to a pentacoordinated Zn-BChl in the B_A-site. This difference in coordination state between the cofactors in the B_A and H_A sites of the Zn-RC was proposed to result in a downhill energy landscape enabling efficient ET and avoiding the deficiency observed in the β mutant RC wherein both B_A- and H_A-sites the BChls are penta-coordinated.[16]

To test the hypothesis that the coordination state of the H_A-cofactor tunes the Zn-RC ET rate and efficiency, we modified one amino acid at position 214 of the M protein (M214) in the RC H_A-site so that a His was present in place of the usual Leu; see Figure 1B. This change is the same as in the original β mutant RC, producing what we call the Zn-β-RC. It was expected that a His residue at this position would provide a fifth ligand to the Zn^{2+} of Zn-BChl in the H_A-site and make it penta- instead of tetra-coordinated. By analogy with the original β mutant RC, the predicted effect of this change would be a 2-fold reduction to the ET time compared to the unmodified Zn-RC.[12]

In contrast to the above prediction, using spectral hole burning (HB),[10,11,18] we demonstrate that both the Zn-RC and Zn-β-RC have surprisingly similar P870* decay times. However, the quantum yield of charge separation in Zn-β-RC decreases by 60% in comparison to Zn-RC. We argue that the decrease in the quantum yield is related to the difference in coordination state of the Zn-BChl in the H_A-site of the RC, as suggested in a previous work.[16] Using high resolution photochemical HB spectra we show, for the first time, that P870 heterogeneity can be measured experimentally. From the simultaneous fit of photochemical (resonant and nonresonant) HB and absorption spectra of P870 we find that electron−phonon coupling parameters in Zn-β-RC and Zn-RC are slightly different. In contrast to earlier simulations,[19−22] we used experimentally determined heterogeneity and a more accurate phonon line shape function to fit various optical spectra, providing more reliable electron−phonon coupling parameters. We also suggest that the shoulder observed on the low energy side of the B Q_y-band, near 820 nm in low temperature absorption and HB spectra of the *Rb. sphaeroides* RC, which is often assigned in the literature to P_+[21,22] (i.e., the upper excitonic component of the homodimer special pair) is likely to originate from an electrochromic shift of the B_B cofactor.

2. MATERIALS AND METHODS

2.1. Bacterial Strains, Plasmids, and Growth of Cultures. *Rb. sphaeroides* strains were grown as described

dx.doi.org/10.1021/jp300304r | J. Phys. Chem. B 2012, 116, 3457−3466

previously[23] at 30 °C in LB medium. Antibiotics were used in *Rb. sphaeroides* cultures at the following working concentrations: spectinomycin 50 μg/mL, tetracycline 2 μg/mL.

2.2. RC Isolation. Cell lysis and membrane isolation were performed as described previously.[23] Briefly, a *Rb. sphaeroides* culture was pelleted at 3000 RCF at 4 °C for 15 min. The supernatant was removed, and a cell pellet was resuspended in a solution of 10 mM Tris-HCl, 150 mM NaCl, and 2 mM $MgCl_2$ (pH 8.0). Cells were disrupted in a modified French press[23] and membranes isolated by ultracentrifugation at 355 040 RCF for 20 min. Membrane pellets were resuspended in 10 mM Tris-HCl and 150 mM NaCl, and isolation of RCs from purified membranes was performed as described previously.[24]

2.3. Construction of ΔRCLH/Δ*bchD* Strain. Chromosomal DNA from wild type *Rb. sphaeroides* strain NCIB8253 was purified from cells and used as a template for PCR amplification of the *bchD* gene using primers *bchD* forward (5′-AAGACGCCGAACACCGTGCTG-3′) and reverse (5′-GCCTGCCCCAGAAGGAGCTC-3′) and the following parameters: platinum Pfx polymerase (Invitrogen) with 7% dimethylsulfoxide and initial denaturation of 94 °C for 5 min, followed by 10 cycles of 94 °C for 15 s, 72° to 67 °C (−0.5 °C per cycle) touchdown for 30 s, 72 °C for 1 min 29 s, followed by 20 cycles of 94 °C for 15 s, 63 °C for 30 s, 72 °C for 1 min 29 s, then 7 min at 72 °C. The PCR product was a 1485 bp section of chromosome 1 that corresponds to the coordinates 1,998,332 to 1,999,721 of NCBI Reference Sequence NC_007493.1. This section encompasses a 254 bp region of the 3′ end of the *bchI* gene, starting 72 bp upstream of a native *SacI* site, and runs 1231 bp into the 5′ end of the *bchD* gene. This region also includes a native *NruI* site at coordinate 1,999,093. The reverse primer that binds within the *bchD* gene was engineered to introduce a *SacI* site through a single mismatch.

The PCR product was cut with *SacI* and ligated into pUC19. The resulting construct was called pUC19(*bchD*). A 2.0 kb *Sma*I fragment containing the Ω cartridge (which encodes spectinomycin-resistance) was cut out of the plasmid pHP45Ω and gel-purified. The pUC19(*bchD*) plasmid was cut with *NruI* and the *Sma*I Ω fragment was blunt ligated into the blunt cut *NruI* site. The resulting construct was called pUC19(*bchD*Ω). Plasmid pUC19(*bchD*Ω) was digested with *SacI*, and the *bchD*Ω insert was gel-purified. The *bchD*Ω *SacI* fragment was ligated into pNHG1. The resulting plasmid was called pNHG1(*bchD*Ω) and was conjugated into *Rb. sphaeroides* strain ΔRCLH.[23] Selection for single-crossovers of pNHG1-(*bchD*Ω) into the chromosome was followed by aerobic growth on spectinomycin-supplemented RCV liquid medium for 5−7 days and then by plating on RCV agar supplemented with spectinomycin and 15% sucrose to counterselect for loss of the pNHG1 plasmid from the chromosome. The confirmed exconjugant was called ΔRCLH/Δ*bchD* and had a RC^- $LH1^+$ $LH2^-$ $bchD^-$ phenotype, confirmed by absorption spectroscopy of isolated membranes and absorption spectra of acetone/methanol extractions. Finally, the plasmid was conjugated into the ΔRCLH/Δ*bchD* strain to yield the ΔRCLH/ΔBchD strain with the phenotype of $RC^+LH1^+LH2^-$ $bchD^-$, confirmed as described above.

2.4. Spectroscopic Measurements. A detailed description of our HB setup can be found in refs 25 and 26. Briefly, low-temperature absorption and HB spectra were recorded with a Bruker HR125 Fourier transform spectrometer at a resolution of either 4 cm^{-1} or 1 cm^{-1}. Nonresonant HB was performed with the green 496.5 nm line from a Coherent Innova 200 Ar^+ ion laser. A tunable (890−905 nm range) coherent CR899 Ti-Sapphire laser (line width of 0.07 cm^{-1}), pumped by 532 nm Spectra-Physics (Millenia 10s) diode laser, was used for resonant photochemical HB. The intensity of the CR899 laser beam was stabilized electro-optically (Brockton Electro-Optics Corp., LPC) and was attenuated (if needed) using a set of neutral density filters. The sample temperature was maintained at 5 K using a Janis 8-DT Super Vari-Temp liquid helium cryostat. The temperature was stabilized and measured with a Lakeshore Cryotronic model 330 temperature controller. For absorption measurement, samples suspended in buffer solution (containing 10 mM Tris-HCl, 1 mM EDTA, pH 8.0, and 0.025% LDAO detergent) were mixed with 70% glycerol (v/v) to make transparent glass when frozen. The optical density of the sample around 800 nm at 5 K was ∼1. The photochemical (transient) HB spectra are obtained by taking the difference of absorption spectra measured with burning laser on and off after the nonphotochemical hole burning (NPHB) is complete. However, in the case of BRCs persistent NPHB is negligibly small.

3. RESULTS

3.1. Low-Temperature Absorption Spectra. Low-temperature absorption spectra of the Zn-RC (red curve a) and Zn-*β*-RC (blue curve b) Q_y region are shown in Figure 2A.

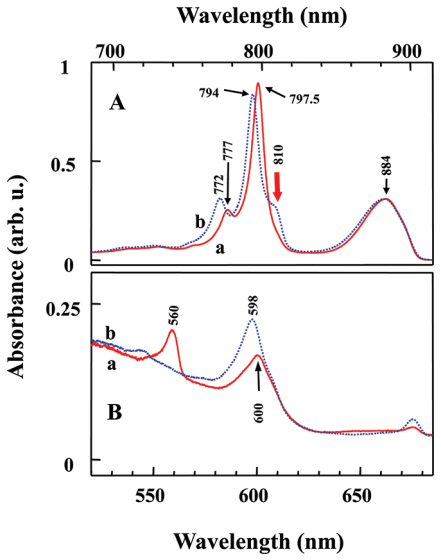

Figure 2. Absorption spectra of RCs at 5 K. The Q_y and the Q_x-regions are shown in frames A and B, respectively. Curves a are of the Zn-RC and curves b the Zn-*β*-RC. Spectra are normalized at the maximum of P870 band.

Spectra a and b are normalized to the same intensity of the P Q_y-band (Q_y transition of $P_{A,B}$ Zn-BChls). The peak of the $P_{A,B}$ Q_y-band at T = 5 K appears near 884 nm, but to be consistent with literature[11,19,20,22] data we refer to this band as P870. In comparison to the Zn-RC, the B Q_y (Q_y transitions of the $B_{A,B}$ Zn-BChls, near 794 nm) and H Q_y (Q_y transitions of $H_{A,B}$ Zn-BChls, near 772 nm) bands in the Zn-*β*-RC are blue-shifted by ∼55 and ∼80 cm^{-1}, respectively. Also note the increase in intensity of the H band and decrease in the B band in the Zn-*β*-RC. The P870 band of the Zn-*β*-RC shows a slight broadening. The red-shifted P870 band in both the Zn-RC and Zn-*β*-RC

dx.doi.org/10.1021/jp300304r | J. Phys. Chem. B 2012, 116, 3457−3466

compared to the B and H bands is caused by electron-exchange (short-range) effects.[27] As was reported for the original β mutant RC[16] the absorption spectrum of the Zn-β-RC shows a distinct shoulder (Figure 2, see red solid arrow in frame A) near 810 nm. The possible origin of this shoulder will be discussed in section 4.1, but at this point we hasten to add that the intensity of this shoulder, even in the WT-RC (which appears near 820 nm at 5 K), varies from sample to sample[16,20,21,28,29] and is almost absent in the R-26[21,30,31] mutant RC (i.e., the RC of the carotenoid-less mutant of *Rb. sphaeroides*), suggesting that in some samples carotenoid (Car) can be lost during isolation/purification procedures. In comparison to the P870 band of the WT-RC[16,21,28] the P870 band of the Zn-RC (at 5 K) is blue-shifted by ~150 cm^{-1}. This shift is caused by the different light-absorption properties of Zn-BChl and (Mg-) BChl.

The Q_x spectral region of two RCs also shows some differences, as illustrated in Figure 2B. As suggested in ref 16 the Q_x-transitions of the Zn-RC $B_{A,B}$ and $P_{A,B}$ Zn-BChls, which are believed to be penta-coordinated, lie near 600 nm. However the band at ~560 nm, which in the Zn-RC arises from the Q_x-transition of tetra-coordinated Zn-BChls in $H_{A,B}$ sites,[16] completely disappears from the Zn-β-RC absorption spectrum, while the intensity near 600 nm (on the high-energy, blue side) increases. Interestingly, the above-mentioned decrease and increase nearly cancel, suggesting that changes occurred at both the H_A and the H_B site (vide infra). Because the Zn-β-RC was thought to have single H_A site point mutation, this behavior is unexpected as the absorption spectra are what would be expected if the Zn atoms of both the $H_{A,B}$ cofactors in Zn-β-RC were penta-coordinated. However, this mutant had an unexpected second site mutation of L86 Q to H. To confirm that this minor mutation (i.e., L86 Q to H) is not associated with the complete disappearance of the $H_{A,B}$ Q_x band mentioned above, another Zn-β-RC (with only the M214L to H mutation) was prepared and studied. We hasten to add that DNA sequencing, performed on both the Zn-RC and Zn-β-RC genes, confirmed that M214 was converted to H. However, optical spectra of both Zn-β-RC samples were nearly indistinguishable, proving that the second site mutation (L86 Q to H) did not affect optical spectra of the RC cofactors (data not shown).

3.2. Nonresonant Photochemical HB (PHB) Spectra. The mainframe in Figure 3 shows Q_y absorption spectra of the Zn-RC measured without (curve a) and with (curve b) burn laser on after the nonphotochemical HB (hole depth less than 1%) is complete. The difference spectrum (b−a) shown as curve c corresponds to the transient photochemical HB (PHB) spectrum. Spectra a, b, and c shown in the lower and upper insets correspond to the Q_x and vibronic spectral regions, respectively. The spectral changes observed in spectrum b (mainframe) are due to formation of charge-separated transient species, that is, $P^+BHQ_A^-$. The formation of $P^+BHQ_A^-$, which lasts for ~100 ms,[16] leads to a bleach of P870 band and a shift of transition frequencies of $B_{A,B}$ and $H_{A,B}$ Zn-BChls, as illustrated by curve c of the mainframe. This electric field-induced spectral band shift in the 750−820 nm region was previously observed in BRCs and is referred to as *electrochromic shift*.[20,21,28,32] As shown in the upper inset, there is also a shift in vibronic transition frequencies. Since the vibronic bands ~730 and ~754 nm (corresponding to vibrational frequencies of ~1150 and ~720 cm^{-1}, respectively) shift to shorter wavelengths in concert with the B band, they are assigned to

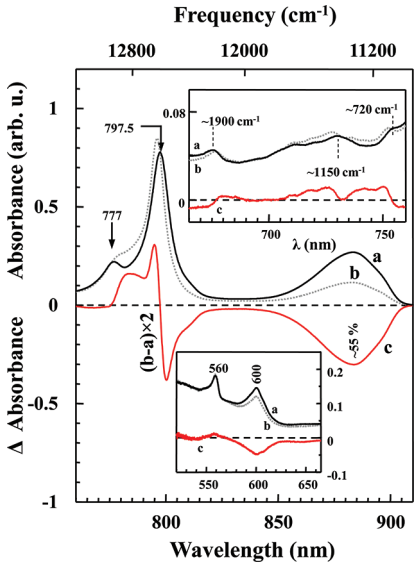

Figure 3. Absorption and nonresonant photochemical HB spectra of the Zn-RC. Curves a and b in the mainframe and both insets correspond to a preburn absorption spectrum and absorption spectrum measured with burn laser on, respectively. For clarity, the Q_x- and vibronic-regions are shown separately in the lower and upper insets. Curves c (multiplied by a factor of 2) are transient PHB spectra obtained with the burn wavelength of 496.5 nm and intensity (I) of 300 mW/cm^2.

the vibrational frequencies of $B_{A/B}$ Zn-BChls. Interestingly, similar modes are observed for BChl in solution.[33,34] In contrast, the weak feature at ~675.5 nm shifts "red" in concert with the H band, but the frequency of ~1900 cm^{-1} (from the H band) is too large and too intense to correspond to a vibrational mode of $H_{A,B}$ Zn-BChls. The presence of this small feature is not critical to the interpretation of our data and most likely originates from a small sample contamination. This is supported by the fact that the intensity of this band was weakly sample-dependent.

The Zn-RC transient PHB spectrum in the Q_x spectral range (Figure 3, curve c, lower inset) is dominated by a bleach of Q_x transition corresponding to the $P_{A/B}$ chlorophylls. However, a small contribution from an electrochromic shift of $H_{A,B}$ and $B_{A,B}$ Zn-BChls cannot be ruled out. Under our current experimental conditions, the P870 bleach in curve c is ~55%, as shown in the mainframe of Figure 3.

The mainframe in Figure 4 shows the Q_y absorption spectrum of the Zn-β-RC measured without (curve a) and with (curve b) the burn laser on after the nonphotochemical hole burning was complete. The difference spectrum c (b−a) corresponds to the transient PHB spectrum. The Q_x and vibronic spectral range of the spectra a, b, and c are shown in the lower and upper insets, respectively. As in the case of the Zn-RC, the formation of $P^+Q_A^-$ results in: (1) P870 band bleaching; (2) an electrochromic shift of the Q_y transition frequency of $B_{A,B}$ (blue shift) and $H_{A,B}$ (red shift) Zn-BChls, as shown by curve c of the mainframe; and (3) shifts of vibronic transition frequencies (see upper inset). Again, vibrational modes of ~1150 and ~720 cm^{-1} (from the B band) shift blue in concert with the B band, therefore, these frequencies most likely belong to the $B_{A,B}$ Zn-BChls. Under similar experimental conditions as those used for the Zn-RC, the bleaching of the P870 band in the Zn-β-RC was ~33%. Assuming similar lifetimes of $P^+Q_A^-$ in both RCs, the decreased yield of $P^+Q_A^-$

dx.doi.org/10.1021/jp300304r | J. Phys. Chem. B 2012, 116, 3457−3466

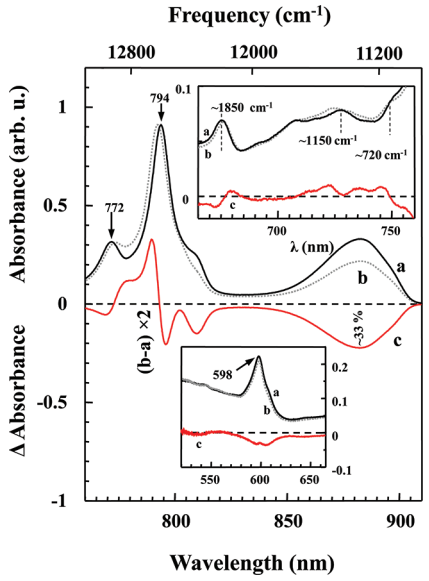

Figure 4. Absorption and nonresonant photochemical HB spectra of the Zn-β-RC. Curves a and b in the mainframe and both insets correspond to a preburn absorption spectrum and absorption spectrum measured with burn laser on, respectively. For clarity, the Q_x- and vibronic-regions are shown separately in the lower and upper insets. Curves c (multiplied by a factor of 2) are transient photochemical HB spectra obtained with the burn wavelength of 496.5 nm (I = 300 mW/cm^2).

formation in the Zn-β-RC could be associated with an increased rate of charge recombination of the $P^+H_A^-$ state in the Zn-β-RC, as suggested for the original β-RC in ref 12. We hasten to add that the % hole depth of the saturated nonphotochemical HB spectrum (data not shown) in both the Zn-RC and Zn-β-RC was less than 1% due to very efficient charge separation in both samples.

Similar to the Zn-RC, the Zn-β-RC transient PHB spectrum in the Q_x region (Figure 4, spectrum c in lower inset) is dominated by Q_x bleaching of the $P_{A,B}$ Zn-BChls, with a small contribution from electrochromic shifts of both the B and H bands. However, there are two obvious differences in the transient PHB spectra of the Zn-β-RC (spectrum c in mainframe of Figure 4) compared to the Zn-RC spectrum shown in Figure 3. The bleaching at ~810 nm which in absorption corresponds to the shoulder on the low energy side of the B band (often assigned in the literature[21,22,32] to the upper excitonic component of the special pair, i.e., P_+) is more pronounced in the Zn-β-RC, and the H-band spectral changes around 772 nm, as expected, are very different. The underlying reasons for these observed differences are discussed in detail in section 4.2.

3.3. Photochemical HB Spectra of P870 and Theoretical Fits. In the low temperature limit, the HB spectrum is defined by $\Delta A = A_t(\Omega, t) - A_{t=0}(\Omega)$, where $A_{t=0}(\Omega)$ is the preburn absorption spectrum, and

$$A(\Omega, t) = \int d\omega L_A(\omega - \Omega) N(\omega) \exp(-P\sigma\varphi L_A(\omega_B - \omega)t) \quad (1)$$

is the postburn absorption spectrum.[11,35] In eq 1 ω_B is the burn/excitation frequency, P is the photon flux, σ and φ are the integrated absorption cross-section and HB quantum yield, respectively, t is the burn time, and $N(\omega)$ is the preburn site distribution function (SDF), describing the probabilities of encountering different zero-phonon transition frequencies, and $L_A(\omega)$ is the single site absorption profile. In the low-fluence limit, the exponent in eq 1 can be expanded in a Taylor series to obtain

$$A(\Omega, t) \approx A(\Omega, 0) - tP\sigma\phi \int d\omega L_A(\omega - \Omega) N(\omega) L_A(\omega_B - \omega) \quad (2)$$

Within the Franck–Condon approximation for an absorptive transition linearly coupled to a harmonic bath, the single site absorption profile can be expanded in terms of R-phonon profiles

$$L_A(\omega; T) \propto e^{-S(T)} \sum_{R=0}^{\infty} \frac{S(T)^R}{R!} l_R(\omega; T) \quad (3)$$

where $l_0(\omega;T)$ is a delta function representing the absorptive zero-phonon line (ZPL), $l_1(\omega;T)$ is a normalized and temperature-weighted spectral density, and for $R > 1$, $l_R(\omega;T)$ is the convolution of $l_1(\omega;T)$ with itself $R - 1$ times. In this description, $l_R(\omega;T)$ represents the contribution of R-phonon transitions to the absorption spectrum (both creation and annihilation). More precisely, if $J(\omega)$ is the transition spectral density, then we define a temperature-weighted density

$$p(\omega; T) = (1 + n(\omega; T))J(\omega) + n(-\omega; T)J(-\omega) \quad (4)$$

which accounts for transitions involving both creation (positive frequencies) and annihilation (negative frequencies) of lattice phonons; the weighting factor $n(\omega;T)$ here is the thermal occupation number of a phonon of frequency ω. The temperature-dependent effective Huang–Rhys factor $S(T)$ is given by

$$S(T) = \int_{-\infty}^{\infty} p(\omega; T) d\omega \quad (5)$$

providing a normalized one-phonon profile

$$l_1(\omega; T) = S(T)^{-1} \cdot p(\omega; T) \quad (6)$$

Note that in the low-temperature limit, $p(\omega;T) \approx J(\omega)$, and the effective factor $S(T)$ reduces to the usual Huang–Rhys factor S defined as the integrated area of the spectral density $J(\omega)$.

For the calculations presented here, the higher-order profiles $l_R(\omega;T)$ were obtained by numerical convolution of the one-phonon profile with itself ($R - 1$ times) and with the ZPL; the sum was truncated after a number of terms sufficient to account for 99.99% of the total intensity of the phonon-sideband (PSB). Finally, to account for the lifetime broadening of the transition, the line shape function $L_A(\omega)$ given by eq 3 was convolved with a Lorentzian line shape function before evaluating eq 2. This approach should be compared with the mean phonon approximation used in earlier calculations,[11,19,20,22] where the spectral density was split into multiple effective phonon densities and the continuous weighting factor $n(\omega;T)$ was replaced by an effective factor $n(\omega_k;T)$ evaluated at a "mean" phonon frequency ω_k near the peak of the k^{th} phonon density; and where in place of numerical convolutions, multiphonon transitions were described simply as increasingly broadened Gaussian/Lorentzian profiles. The current approach (the absorptive equivalent of the fluorescence line shape functions used in ref 36) is more direct and describes the phonon line shape more accurately.[10] On the basis of previous works,[20–22]

dx.doi.org/10.1021/jp300304r | J. Phys. Chem. B 2012, 116, 3457–3466

only two profiles corresponding to peak frequencies ω_{ph} and ω_{sp} are required to simultaneously fit the absorption and λ_B-dependent PHB spectra of P870. Consistent with an earlier assignment, we refer ω_{ph} to the mean (or rather peak) phonon frequency and ω_{sp} to the special pair marker mode.[11,19,20,22] Special pair marker modes are intermolecular vibrational modes localized on the special pair.[21,22] As before,[11,19,20,22] line shape for ω_{ph} mode is described by a Gaussian (fwhm = Γ_G^{ph} cm^{-1}) and Lorentzian (fwhm = Γ_L^{ph} cm^{-1}) on the low and high energy sides, respectively. As suggested in refs 19 and 21, Lorentzian line shape (fwhm = Γ_L^{sp} cm^{-1}) is used for ω_{sp} mode. However, in contrast to previous work, the special pair and phonon densities were combined into a single spectral density $J(\omega)$ before the evaluation of eq 3, taking into account mixed transitions (e.g., multiphonon transitions involving creation or annihilation of phonons from both profiles) directly and with no additional approximations.

The experimental PHB spectra (black solid curves) of P870 and fits (red curves) for the Zn-RC and Zn-β-RC are shown in Figure 5A and B, respectively. Note a very good agreement

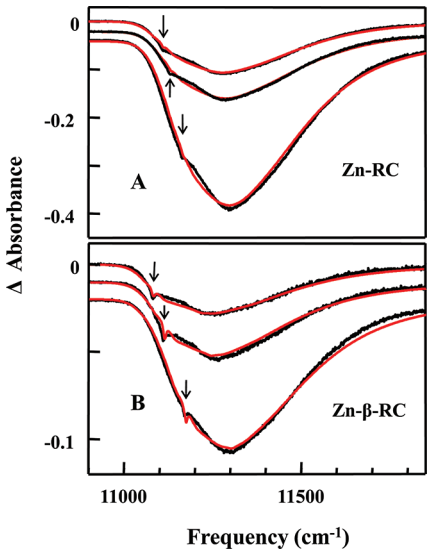

Figure 5. Comparison of calculated and experimental transient spectra. Black solid curves in Frames A and B show experimental photochemical HB spectra of P870 for Zn-RC and Zn-β-RC, respectively. Calculated spectra are shown in red. Solid arrows in both frames refer to laser burn frequencies (ω_B) and correspond to 11111, 11131, and 11164.6 cm^{-1} (top to bottom) in Frame A, and 11082, 11112, and 11172.3 cm^{-1} (top to bottom) in Frame B, respectively. See Table 1 for fitting parameters.

between experimental curves and their fits. Unlike in earlier modeling studies[19−22] experimentally determined inhomogeneous broadening has been used in this work. The parameters obtained from the simultaneous fit of absorption and multiple PHB spectra of P870 for two samples are summarized in Table 1. The total Huang−Rhys (HR) factor is defined as $S_t = S_{ph} + S_{sp}$, where S_{ph} and S_{sp} are HR factors corresponding to ω_{ph} and ω_{sp} modes, respectively. The total HR factors/reorganization energy ($= \Sigma_i S_i \omega_i$) for Zn-RC and Zn-β-RC are 4.6/238 and 3.6/188, respectively. The weaker el-ph coupling in Zn-β-RC is consistent with more pronounced ZPH in experimental PHB spectra. The presence of strong el-ph coupling in RCs studied in this work suggests that P870 possesses a significant charge transfer (CT) character with the lowest-energy absorption band largely homogeneously broadened. However, the parameters obtained for the Zn-RC and Zn-β-RC are not directly comparable to the *Rb. sphaeroides* WT-RC[21] because our RCs contain Zn-BChls instead of BChls. However, the above-mentioned difference in el-ph coupling between RCs with Zn-BChls (this work) and BChls is likely real, as in this work we used the experimentally determined SDF, and the line shape functions used previously[35] and often used in the literature[11,19−22] carry an improper dependence on the number of phonons involved in the transition; corrected equations will be published elsewhere [Reppert et al., to be submitted]. Here we only mention that el-ph coupling strengths for Zn-RC and Zn-β-RC calculated in this work are about 50% and 40% larger, respectively, than those calculated with the same parameters but the line shape function from ref 35. We anticipate that a recalculated el-ph coupling strength for the *Rb. sphaeroides* WT-RC (to be published elsewhere) using our approach will also be larger than the S_t of 3.3 reported in ref 21.

3.4. Zero Phonon Hole (ZPH) Action Spectra and Electron Transfer Times. ZPH action spectroscopy allows the investigation of the lowest energy state(s) as well as determination of inhomogeniety of various molecular systems[10,25,26,37−39] embedded in a glassy matrix at low temperatures. In ZPH action spectroscopy (in absorption mode), the burn wavelength (λ_B) dependence of *nonphotochemical* ZPH depth is probed under a constant irradiation dose, that is, a constant fluence. Fluence is defined as $f = I \times t$, where I is laser intensity and t is irradiation time. But here, for the first time, we have attempted to extract ZPH action spectra by probing burn wavelength (λ_B) dependence of *photochemical* ZPH depth under constant laser intensity. This allows us to find the inhomogeneous broadening (Γ_{inh}) of the lowest-energy charge separating state.

In Figure 6 the black solid curves in frame A (Zn-RC) and frame B (Zn-β-RC) show the experimental absorption spectra of P870. Fits to the absorption spectra, hardly distinguishable from experimental spectra, are shown as red curves. The equations used to simultaneously describe both absorption and PHB spectra were given in section 3.3. The sharp blue spikes in the 11000−11250 cm^{-1} frequency region shown in frames A and B are the inverted ZPH spectra for the Zn-RC and Zn-β-RC, respectively. These inverted sharp ZPH are obtained by fitting Lorentzian curves to the ZPH and subtracting broad contributions from the transient PHB spectra of P870

Table 1. Electron-Phonon Coupling Parameters for P870 in Zn-RC and Zn-β-RC

	ω_{ph} (cm^{-1})	Γ_G^{ph} (cm^{-1})	Γ_L^{ph} (cm^{-1})	$S_{ph} \pm 0.1$	ω_{sp} (cm^{-1})	Γ_L^{sp} (cm^{-1})	$S_{sp} \pm 0.1$	$S_t \pm 0.1$	$\Sigma_i S_i \omega_i \pm 4$
Zn-RC[a,b]	30	25	25	3.6	130	25	1.0	4.6	238
Zn-β-RC[a,b]	30	30	50	2.8	130	25	0.8	3.6	188

[a]SDF peak/width of 11120/110 cm^{-1} (black solid curve in Figure 6 frame A) and 11140/140 cm^{-1} (black solid curve in Figure 6 frame B) were used for Zn-RC and Zn-β-RC, respectively. [b]Γ_{hom} of ∼5 cm^{-1} (fwhm) was used for both samples which is very close to average half width half-maximum of experimental ZPH; ph = phonon, sp = special pair, t = total.

dx.doi.org/10.1021/jp300304r | J. Phys. Chem. B 2012, 116, 3457−3466

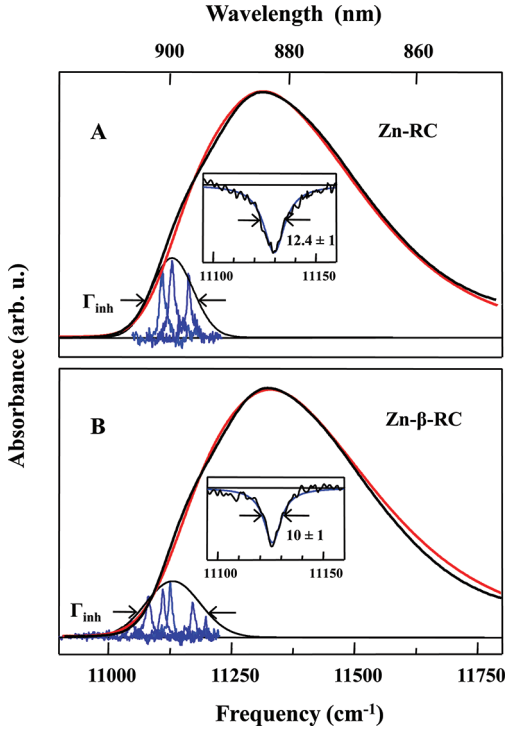

Figure 6. Zero phonon hole (ZPH) action spectra analysis of Zn-RC and Zn-β-RC. Frames A and B show experimental P870 absorption band (black solid curves) of Zn-RC and Zn-β-RC, respectively. Calculated absorption spectra are shown in red. The blue color sharp spikes in both frames (in the ~11000−11250 cm^{-1} region) show the inverted ZPHs. The ZPHs were measured under identical conditions (I = 250 mW/cm^2, read resolution = 1 cm^{-1}). The insets show a magnified view of the experimental (black) ZPHs obtained with the burn wavelength (λ_B) of 898.4 nm (ω_B = 11131 cm^{-1}) and 898.7 nm (ω_B = 11127 cm^{-1}) for Zn-RC (frame A) and Zn-β-RC (frame B), respectively. The Lorenzian fits of the ZPHs are shown in blue.

measured at different λ_B under constant laser intensity. Representative ZPHs with Lorentzian fits are shown in the insets of Figure 6. Solid black curves in frame A (Zn-RC) and B (Zn-β-RC) represent the Gaussian distribution of ZPHs with inhomogeneous broadening (Γ_{inh}) of 110 ± 10 cm^{-1} and 130 ± 10 cm^{-1}, respectively. These curves provide the SDF of the primary donor state (P870) in the Zn-RC and Zn-β-RC. Each sharp spike in both frames can be fitted with a Lorentzian profile, as it reflects the homogeneous line width (i.e., Γ_{hom} = 1/2 ZPH width[10,11,18]). A weakly λ_B-dependent ZPL width ranging from 9 to 11 cm^{-1} is obtained for both samples. The ET time is obtained from Γ_{hom} using eq 7[10,11,18]

$$\Gamma_{hom}(cm^{-1}) = (1/2\pi cT_1 + 1/2\pi c\tau_{ET}) + 1/\pi cT^*_2 \approx 1/2\pi c\tau_{ET} \quad (7)$$

where T_1 is the fluorescence lifetime, T_2* is the "pure" dephasing time, which at (T = 5 K) is very large in comparison to T_1, c is the velocity of light in (cm s^{-1}), and τ_{ET} is the electron transfer time. Equation 7 provides τ_{ET} since the latter is $\ll T_1$. Our data reveal the both Zn-RC and Zn-β-RC have an average ET time of ~1 ps.

4. DISCUSSION

4.1. Low-Temperature Absorption Spectra. It was previously established that in the WT-RC the Q_y transitions of the H_A and B_A cofactors lie at higher energies than the H_B and B_B cofactor transitions.[27,28,40] This is also true for the Zn-RC and Zn-β-RC, because the interpigment distance and orientation should not be altered from the WT-RC. Excitonic calculations[21,27,41] showed that nearest neighbor V_{nm} coupling (i.e., B_A−H_A and B_B−H_B coupling) is in the range of 100−200 cm^{-1}. This has been confirmed by the recent two color three pulse phonon echo peak shift spectroscopy, which directly measured the B−H coupling of 170 ± 30 cm^{-1}.[42] In the absence of a crystal structure of the Zn-RC and Zn-β-RC (research in progress), the coupling constants cannot be calculated at the present time, however, the B−H coupling in the Zn-RC should not alter much from that observed in the WT-RC.

It has been established that the Q_x transition of metalloporphyrins is more sensitive than the Q_y transition to the coordination state of the metal center.[43] For example, the Q_x/Q_y transitions of Zn-BChl *a* in solution at room temperature lie at ~560/760 nm (tetra-coordinated) and 580/770 nm (penta-coordinated).[43] Therefore, it appears that in solution a change from tetra- to penta-coordination of Zn-BChl results in a relatively large red shift of both the Q_x- and the Q_y-transitions. In the case of the Zn-β-RC, the change from tetra- to penta-coordination of Zn-BChl in the H_A site results in a red shift of the H band Q_x-transition, but the Q_y-transition shifts to the blue, along with the B Q_y-band (Figure 2A, curve b). The blue shift of both the B and H Q_y-bands in the absorption spectrum of the Zn-β-RC most likely originates from a modification of excitonic interaction (due to modified pigment site energies) induced by the tetra- to penta-coordination change of the H_A site Zn-BChl. Such a correlated blue shift of both the H and the B Q_y-bands might contribute to the efficient H to B excitation energy transfer (EET) in the Zn-β-RC. Figure 2B shows that mutation of the M214 residue from Leu to His results in about a 38 nm red shift in the Q_x transition wavelength of the H_A Zn-BChl. This observation is similar to that previously reported[44] where a change from penta- to hexa-coordination of the B_B BChl in the WT-RC resulted in a red shift of Q_x transition (at 77 K) of about 31 nm. Because, as stated earlier, the 560 nm band belongs to Q_x transitions of both $H_{A,B}$ cofactors, one would expect that the intensity of this band should decrease only by half, as only the H_A site was intentionally modified. It is puzzling that this band disappears completely. In the absence of a high resolution crystal structure of both the Zn-RC and Zn-β-RC, at the present time we only can offer three tentative explanations:

(1) *Both the Zn-RC and Zn-β-RC lack an H_B cofactor.* Our optical spectra suggest that the Zn-RC and Zn-β-RC may assemble without the H_B cofactor and/or during the isolation procedure this cofactor is lost. The latter possibility cannot be excluded, as it was shown in literature[45] that the mutation of the M149 residue from Ala to Trp in the *Rb. sphaeroides* RC led to an RC lacking the H_B (BPhe) cofactor. Interestingly, in that mutant[45] the time constants of active branch charge separation were not altered, as observed in the case of the Zn-RC and Zn-β-RC. A similar conclusion was reached for L185 Leu to His mutant,[45] where the H_B BPhe was replaced with BChl. For example, if the absorption spectrum of the M149 Ala to Trp mutant reported in Figure 4a of ref 45 is compared to the absorption spectrum of the Zn-RC shown in Figure 2 of this work, two similar spectral

dx.doi.org/10.1021/jp300304r | J. Phys. Chem. B 2012, 116, 3457−3466

features are revealed. In both cases, unlike in the WT-RC, the $H_{A,B}$ Q_x-band does not split, and the shoulder on the low-energy side of the B Q_y-band is absent. In addition, careful examination of many low-temperature absorption spectra of *Rb. sphaeroides* WT-RCs reported in the literature[20,21,28−31] leads us to conclude that the distinct shoulder near 820 nm (at 5 K in the *Rb. sphaeroides* WT-RC) is present only in some, that is, the best RC preparations most likely (see below) that retain the Car. We suggest that this shoulder near 820 nm belongs to the Q_y transition of the B_B BChl. This is because B_B is close to the Car and H_B, and so a possible loss of BChl from the H_B site (as in the M149 Ala to Trp mutant[45]) or loss of Car (as in the R-26 mutant[21,30,31]) would give the B_B band a more monomeric character. This could lead to a blue shift of the Q_y transition wavelength of B_B, resulting in disappearance of the 810−820 nm shoulder (at ∼810 nm in the Zn-RC and ∼820 nm in the WT-RC). These two observations (i.e., the absence of a 810 nm shoulder on the lower energy side of the B Q_y-band and the absence of H Q_x-band splitting) could suggest that Zn-RC and Zn-*β*-RC lack the H_B BChl. The absence of the H_B BChl would explain why the H Q_x-band near 560 nm completely disappears in the Zn-*β*-RC (see Figure 2B). We suggest that the intensity of the H Q_y-band in the Zn-RC and Zn-*β*-RC is too weak (compared to the WT-RC,[16] and assuming a similar oscillator strength of BChl in the WT-RC and Zn-BChl in the Zn-RC) to account for a contribution of two Zn-BChl pigments in the H Q_y-band transitions of the Zn-RC and Zn-*β*-RC. It is also possible that spectral differences observed around the B Q_y-band (including the 810 nm shoulder) are due to the loss of carotenoid in Zn-RCs (see below for further discussion).

(2) *The Zn-β-RC contains two penta-coordinated Zn-BChls, one in the H_B site and one in the H_A site.* The coordination state of these Zn-BChls may be due to two mutations, that is, L185 Leu→His and M214 Leu→His, resulting in penta-coordination of both $H_{A,B}$ Zn-BChls. The observation that the $H_{A,B}$ Q_x-band at ∼560 nm completely disappears with a concomitant increase in intensity of the Q_x-band at ∼600 nm supports this idea. Alternatively, it cannot be excluded that the H_B Zn-BChl (in both the Zn-RC and Zn-*β*-RC) is ligated by an intervening water molecule, such that the H_B Q_x transition lies in the range of 590−610 nm and not ∼560 nm. In fact, it was reported that ligation by a water molecule can cause a large (∼31 nm) Q_x shift.[44]

(3) *Redistribution of oscillator strength.* It could be conceived that neither penta-coordination of the H_B Zn-BChl nor its absence explains the differences observed. In this case one must explain the spectral changes observed in both the Q_x and Q_y transitions by considering the redistribution of the oscillator strength between Q_x and Q_y transitions of excitonically coupled $H_{A,B}$ and $B_{A,B}$ chromophores. Although intensity borrowing between Q_y excitonic states is not unusual, point mutation-induced intensity borrowing between Q_x and Q_y transitions, to our knowledge, has not been reported for any RC.

In summary, no final conclusion regarding the number of cofactors can be reached at this point. We suggest that the most likely scenario is given by explanation number 2 (vide supra). The spectral changes between the Zn-RC and the Zn-*β*-RC in the range of 750−820 nm can be explained by considering: (1) mutation-induced changes in the H_A site; (2) the presence of more carotenoid in Zn-*β*-RCs than in the Zn-RCs. However, complete disappearance of the ∼560 nm Q_x band in the Zn-*β*-RC can be explained only by considering that Zn-BChls in $H_{A,B}$ sites are penta-coordinated.

4.2. On the Nature of the 810 nm Shoulder Observed on the Low-Energy Side of the B Q_y-Band in Absorption Spectra of the Zn-RC and Zn-β-RC. There are conflicting opinions regarding the shoulder present on low energy side of the Q_y B-band in BRCs.[20−22,28,32,49] For example, this shoulder (at 5 K) appears at ∼850 in the *Rps. viridis*[22,32] and ∼820 nm in the *Rb. sphaeroides*[20−22,28] WT-RC. Earlier semiempirical[27] and excitonic[46] calculations did not assign this shoulder to the P_+ excitonic component (vide supra). However, on the basis of polarization excitation spectra[47] it was concluded that the shoulder on the low energy side of the B Q_y-band in low-temperature absorption spectra of the *Rps. viridis* RC is an upper excitonic component (P_+) of P960 (the special pair). A similar conclusion was reached on the basis of NPHB experiments on the *Rps. viridis* P960.[32] On the basis of λ_B-dependent PHB spectra of P870[48] it was suggested that the shoulder near 820 nm in the *Rb. sphaeroides* WT-RC has a significant contribution from P_+. Although ref 22 confidently assigns the lower energy side absorption to P_+, our data do not support this assignment. That is, it is not clear why: (1) electron−phonon coupling of the ∼820 nm (in *Rb. sphaeroides*) and/or ∼850 nm (in *Rps. viridis*) bands is very weak in comparison to P870 and P960, respectively; and (2) linear pressure shift of this band is very weak and is similar to that observed for a monomer. Interestingly, low-temperature (5 K) Stark spectra of *Rb. sphaeroides* and the original *β* mutant were interpreted[28] as indicating that P_+ of P870 is near 800 nm (underneath the B Q_y-band but not the 820 nm shoulder) and carries a very small oscillator strength relative to the Q_y transition. This assumption was based on a picosecond circular dichroism study of the *Rb. sphaeroides* RC reported in ref 49. Picosecond photodichroism studies of the *Rb. sphaeroides* RC at 5 K also suggested that the low energy shoulder of B Q_y-band is comprised mainly of one of the two BChls that are not part of P.[50] Thus, there is no general consensus on the origin of the above-discussed shoulder. However, our data support the conclusions reached in refs 28 and 49, as discussed above, that is, the P_+ component in BRCs must be very weak and is obscured by an overlapping B band. Recall, as discussed above, that the variable intensity of this shoulder in various BRCs may indicate the absence of carotenoid and/or lack of the H_B pigment in mutated BRCs. One more indication that the low energy side absorption does not belong to the P_+ excitonic component of the special pair comes from the 77 K absorption spectrum of a M202 His to Leu mutant (the "heterodimer" mutant) reported in ref 51. where it was shown that in absorption spectra of the M202 His to Leu mutant the P870 band is very weak, but the lower energy side of B Q_y-band is as intense as in the WT-RC. Interestingly, in the same paper, the M-side bacteriochlorophyll was changed to a bacteriopheophytin in addition to the heterodimer mutation by the addition of a M182 His to Leu mutation to the M202 mutation. In this mutant, the shoulder seems to disappear completely, suggesting that it is more a property of the accessory bacteriochlorophyll than of the dimer.

Therefore, we conclude that data reported in this work are inconsistent with a previous suggestion[22,48] that the lower energy shoulder observed near 820 nm in the *Rb. sphaeroides* WT-RC within the B Q_y-band in low-temperature transient spectra is an upper excitonic component of P870 (i.e., P_+). If one accepts that the ~810 nm shoulder in the Zn-RC and the well-resolved band near 810 nm band in Zn-*β*-RC are due to P_+, it is hard to see why a simple point mutation makes the shoulder so much stronger in the Zn-*β*-RC (see main frames of Figures 3 and 4). To explain this, one would have to assume that the Leu→His mutation in the H_A site results in a significant change in the relative orientation of transition dipoles of P_A and P_B. This does not seem feasible, and as pointed out earlier, the increase in intensity of the 810 nm shoulder in the absorption spectrum (see curve b in Figure 2, frame A) and the 810 nm band in transient spectrum (curve c, mainframe of Figure 4) in the Zn-*β*-RC must have a different origin, as discussed above.

In addition, our resonant PHB spectra of P870 do not support the idea that the 810 nm shoulder is due to P_+. The resonant PHB spectra of the Zn-*β*-RC burn at the high energy (curve a, black) and low energy (curve b, gray) edges of SDF are replotted in Figure 7 (spectra are normalized to the same

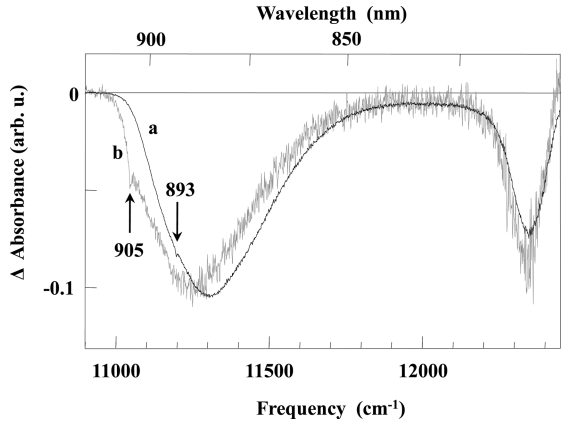

Figure 7. Photochemical HB spectra of P870 for Zn-*β*-RC at λ_B of 893 nm (ω_B = 11198.2 cm^{-1}, spectrum a) and 905 nm (ω_B = 11049.7 cm^{-1}, spectrum b). Spectra are normalized to the same P870 bleach.

intensity of P870 bleaching). Unlike the centroid of the P870 bleach, the bleach at ~810 nm does not shift at all. This shows that the feature at ~810 is not correlated with P870. This again proves that the low energy shoulder near 810 nm in absorption spectrum is not necessarily associated only with P_+. As stated earlier, the major contribution to the low energy shoulder in absorption spectrum comes from B_B. If the transition frequency of B_B is slightly perturbed, for example due to the absence of a nearby carotenoid and/or H_B, the B_B band due to modified excitonic interactions and different composition of various excitonic states could undergo a blue shift leading to decreased intensity of this shoulder. This interpretation is in accord with the variable intensity of 810/820 nm shoulders in low-temperature absorption spectra of various *Rb. sphaeroides* RC samples.[16,20,22,28,31,30] The absence of the low energy shoulder in the absorption spectrum of the Zn-RC shown in Figure 2 may be, as stated earlier, due to loss of carotenoid. Further biochemical studies of Zn-RC and Zn-*β*-RC should confirm or reject this hypothesis.

Finally, we comment on the different shapes of PHB spectra of the Zn-RC (especially in the range 770−820 nm; see Figure 3 curve c in the mainframe) and the Zn-*β*-RC (see Figure 4, curve c in the mainframe). If one accounts for the shift in absorption between the Zn-RC and Zn-*β*-RC, the major changes in the two PHB spectra are observed at ~810 nm (corresponding to the lower energy spectrum of the B Q_y-band) and ~775 nm (H Q_y-band). The more pronounced bleaching at ~810 nm in the Zn-*β*-RC (consistent with more absorption ~810 nm), as stated earlier, is not associated with P_+; we believe that this bleaching comes from an electrochromic shift of B_B. Our findings agree with those of a previous work[28] which showed that a lower effective dielectric constant on the RC B side (i.e., the inactive branch) caused the B branch cofactors (B_B and H_B) to exhibit more electrochromic shift than the A branch cofactors (H_A, B_A).

5. CONCLUSIONS

We have shown that the coordination state of H_A in the Zn-RC does not tune the electron transfer rate. The formation of the $P^+Q_A^-$ state is observed in both the Zn-RC and the Zn-*β*-RC, although under identical experimental conditions a significantly deeper P_ band (corresponding to the lower-energy, special pair, excitonic component) was observed in the Zn-RC than in the Zn-*β*-RC. However, the average (weakly frequency-dependent) low-temperature ET times (measured from ZPHs in resonant transient HB spectra) are comparable (within ~1 ps) and similar to those previously observed in the WT-RC.[48] The ET rates observed in this work for the Zn-RC are in good agreement with recent room-temperature, time-domain data.[16] Additionally, our data indicate, in agreement with ref 28 and 49, that bleaching at ~810 nm is not associated with an upper excitonic component (P_+) of P870 but instead originates from an electrochromic shift of the B_B Zn-BChl. ZPH-action spectra revealed inhomogeneous broadening (Γ_{inh}) of ~110 ± 10 cm^{-1} (Zn-RC) and ~130 ± 10 cm^{-1} (Zn-*β*-RC). Simultaneous fit of the absorption and resonant/nonresonant HB spectra for both types of RC, using experimentally determined Γ_{inh} and properly accounting for mixed transitions (e.g., multiphonon transitions involving creation or annihilation of phonons), provided a total Huang−Rhys factor of 4.6 ± 0.1 for the Zn-RC and 3.6 ± 0.1 for the Zn-*β*-RC, respectively.

AUTHOR INFORMATION

Corresponding Author

*E-mail: ryszard@ksu.edu.

Notes

The authors declare no competing financial interest.

ACKNOWLEDGMENTS

The authors acknowledge the Division of Chemical Sciences, Geosciences, and Biosciences, Office of Basic Energy Sciences of the U.S. Department of Energy through Grant DE-EC9987 (to R.J.) for funding the application of hole-burning spectroscopy to study electron transfer in *Rhodobacter sphaeroides* reaction centers containing Zn-bacteriochlorophyll, and the Canadian Natural Sciences and Engineering Research Council Grant 2796-2008 to (J.T.B.) for the design and preparation of the reaction centers used in these studies.

REFERENCES

(1) Qian, P.; Hunter, C. N.; Bullough, P. A. *J. Mol. Biol.* **2005**, *349*, 948−960.
(2) Scheuring, S.; Busselez, J.; Levy, D. *J. Biol. Chem.* **2005**, *280*, 1426−1431.
(3) Scheuring, S.; Francia, F.; Busselez, J.; Melandri, B. A.; Rigaud, J. L.; Levy, D. *J. Biol. Chem.* **2004**, *279*, 3620−3626.
(4) Yeates, T. O.; Komiya, H.; Chirino, A.; Rees, D. C.; Allen, J. P.; Feher, G. *Proc. Natl. Acad. Sci. U.S.A.* **1988**, *85*, 7993−7997.
(5) Lancaster, C. R. D.; Ermler, U.; Michel, H. In *Anoxygenic photosynthetic bacteria*; Blankenship, R. E., Madigan, M. T., Bauer, C. E., Eds.; Kluwer Academic Publishers: Dordrechet, The Netherlands, 1995; pp 503−526.
(6) Arlt, T.; Schmidt, S.; Kaiser, W.; Lauterwasser, C.; Meyer, M.; Scheer, H.; Zinth, W. *Proc. Natl. Acad. Sci. U.S.A.* **1993**, *90*, 11757−11761.
(7) Jones, M. R. *Biochem. Soc. Trans.* **2009**, *37*, 400−407.
(8) Williams, J. C.; Allen, J. P. In *The purple phototrophic bacteria*; Hunter, C. N., Daldal, F., Thurnauer, M. C., Beatty, J. T., Eds.; Springer Science: Dordrechet, The Netherlands, 2009; pp 337−353.
(9) Woodbury, N. W.; Allen, J. P. In *Anoxygenic photosynthetic bacteria*; Blankenship, R. E., Madigan, M. T., Bauer, C. E., Eds.; Kluwer Academic Publishers: Dordrechet, The Netherlands, 1995; pp 527−557.
(10) Jankowiak, R.; Reppert, M.; Zazubovich, V.; Pieper, J.; Reinot, T. *Chem. Rev.* **2011**, *111*, 4546.
(11) Jankowiak, R.; Hayes, J. M.; Small, G. J. *Chem. Rev* **1993**, *93*, 1471−1502.
(12) Kirmaier, C.; Gaul, D.; DeBey, R.; Holten, D; Schenck, C. C. *Science* **1991**, *251*, 922−927.
(13) Wang, H.; Lin, S.; Allen, J. P.; Williams, J. C.; Blankert, S.; Laser, C.; Woodbury, N. W. *Science* **2007**, *316*, 747−750.
(14) Jaschke, P. R.; Beatty, J. T. *Biochemistry* **2007**, *46*, 12491−12500.
(15) Jaschke, P. R.; Hardjasa, A.; Digby, E. L.; Hunter, C. N.; Beatty, J. T. *J. Biol. Chem.* **2011**, *286*, 20313−20322.
(16) Lin, S.; Jaschke, P. R.; Wang, H.; Paddock, M.; Tufts, A.; Allen, J. P.; Rosell, F. I.; Mauk, A. G.; Woodbury, N. W.; Beatty, J. T. *Proc. Natl. Acad. Sci. U.S.A.* **2009**, *106*, 8537−8542.
(17) Allen, J. P.; Feher, G.; Yeates, T. O.; Rees, D. C.; Deisenhofer, J.; Michel, H.; Huber, R. *Proc. Natl. Acad. Sci. U.S.A.* **1986**, *83*, 8589−8593.
(18) Rebane, K. K.; Rebane, L. A. In *Topics in current physics, Persistent Spectral Hole Burning: Science and Applications*; Moerner, W. E., Ed.; Springer-Verlag: New York, 1987; pp 17−74.
(19) Johnson, S. G.; Tang, D.; Jankowiak, R.; Hayes, J. M.; Small, G. J. *J. Phys. Chem.* **1990**, *94*, 5849−5855.
(20) Johnson, E. T.; Nagarajan, V.; Zazubovich, V.; Riley, K.; Small, G. J.; Parson, W. W. *Biochemistry* **2003**, *42*, 13673−13683.
(21) Lyle, P. A.; Kolaczkowski, S. V.; Small, G. J. *J. Phys. Chem.* **1993**, *97*, 6924−6933.
(22) Small, G. J. *Chem. Phys.* **1995**, *197*, 239−257.
(23) Jaschke, P. R.; Drake, I.; Beatty, J. T. *Photosynth. Res.* **2009**, *102*, 95−97.
(24) Goldsmith, J. O.; Boxer, S. G. *Biochim. Biophys. Acta* **1996**, *1276*, 171−175.
(25) Neupane, B.; Dang, N. C.; Acharya, K.; Reppert, M.; Zazubovich, V.; Picorel, R.; Seibert, M.; Jankowiak, R. *J. Am. Chem. Soc.* **2010**, *132*, 4214−4229.
(26) Dang, N. C.; Zazubovich, V.; Reppert, M.; Neupane, B.; Picorel, R.; Seibert, M.; Jankowiak, R. *J. Phys. Chem. B* **2008**, *112*, 9921−9933.
(27) Warshel, A.; Parson, W. W. *J. Am. Chem. Soc.* **1987**, *109*, 6152−6163.
(28) Steffen, M. A.; Lao, K.; Boxer, S. G. *Science* **1994**, *264*, 810−816.
(29) Meech, S. R.; Hoff, A. J.; Wiersma, D. A. *Proc. Natl. Acad. Sci. U.S.A.* **1986**, *83*, 9464−9468.
(30) Lin, S.; Jackson, J. A.; Taguchi, A. K. W.; Woodbury, N. W. *J. Phys. Chem. B* **1999**, *103*, 4757−4763.
(31) Vos, M. H.; Lambry, J.-C.; Robles, S. J.; Youvan, D. C.; Breton, J.; Martin, J.-L. *Proc. Natl. Acad. Sci. U.S.A.* **1992**, *89*, 613−617.
(32) Reddy, N. R. S.; Kolaczkowski, S. V.; Small, G. J. *Science* **1993**, *260*, 68−71.
(33) Zazubovich, V.; Tibe, I.; Small, G. J. *J. Phys. Chem. B* **2001**, *105*, 12410−12417.
(34) Rätsep, M.; Cai, Z.-L.; Reimers, J. R.; Freiberg, A. *J. Chem. Phys.* **2011**, *134*, 024506/1−024506/15.
(35) Hayes, J. M.; Lyle, P. A.; Small, G. J. *J. Phys. Chem.* **1994**, *98*, 7337−7341.
(36) Acharya, K.; Neupane, B.; Reppert, M.; Feng, X.; Jankowiak, R. *J. Phys. Chem. Lett.* **2010**, *1*, 2310−2315.
(37) Feng, X.; Neupane, B.; Acharya, K.; Zazubovich, V.; Picorel, R.; Seibert, M.; Jankowiak, R. *J. Phys. Chem. B* **2011**, *115*, 13339−13344.
(38) Purchase, R.; Völker, S. *Photosynth. Res.* **2009**, *101*, 245−266.
(39) Neupane, B.; Dang, N. C.; Kelley, R. F.; Wasielewski, M. R.; Jankowiak, R. *J. Phys. Chem. B* **2011**, *115*, 10391−10399.
(40) Huang, L.; Wiederrecht, G. P.; Utschig, L. M.; Schlesselman, S. L.; Xydis, C.; Laible, P. D.; Hanson, D. K.; Tiede, D. M. *Biochemistry* **2008**, *47*, 11387−11389.
(41) Plato, M.; Moebius, K.; Michel-Beyerle, M. E.; Bixon, M.; Jortner, J. *J. Am. Chem. Soc.* **1988**, *110*, 7279−7285.
(42) Parkinson, D. Y.; Lee, H.; Fleming, G. R. *J. Phys. Chem. B* **2007**, *111*, 7449−7456.
(43) Hartwich, G.; Fiedor, L.; Simonin, I.; Cmiel, E.; Schäfer, W.; Noy, D.; Schertz, A.; Scheer, H. *J. Am. Chem. Soc.* **1998**, *120*, 3675−3683.
(44) Frolov, D.; Marsh, M.; Crouch, L. I.; Fyfe, P. K.; Robert, B.; van Grondelle, R.; Hadfield, A.; Jones, M. R. *Biochemistry* **2010**, *49*, 1882−1889.
(45) Watson, A. J.; Fyfe, P. K.; Frolov, D.; Wakeham, M. C.; Nabedryk, E.; van Grondelle, R.; Breton, J.; Jones, M. R. *Biochim. Biophys. Acta* **2005**, *1710*, 34−36.
(46) Knapp, E. W.; Scherer, P. O. J.; Fischer, S. F. *Biochim. Biophys. Acta* **1986**, *852*, 295−305.
(47) Vermeglio, A.; Paillotin, G. *Biochim. Biophys. Acta* **1982**, *681*, 32−40.
(48) Johnson, S. G.; Tang, D.; Jankowiak, R.; Hayes, J. M.; Small, G. J.; Tiede, D. M. *J. Phys. Chem.* **1989**, *93*, 5953−5957.
(49) Xie, X.; Simon, J. D. *Biochim. Biophys. Acta* **1991**, *1057*, 131−139.
(50) Kirmaier, C.; Holten, D.; Parson, W. W. *Biochim. Biophys. Acta* **1985**, *810*, 49−61.
(51) King, B. A.; de Winter, A.; McAnaney, T. B.; Boxer, S. G. *J. Phys. Chem. B* **2001**, *105*, 1856−1862.